IEEE Access
Multidisciplinary ⋮ Rapid Review ⋮ Open Access Journal

Received 21 March 2025, accepted 31 March 2025, date of publication 7 April 2025, date of current version 17 April 2025.

Digital Object Identifier 10.1109/ACCESS.2025.3558700

RESEARCH ARTICLE

UAV Path Planning for Precision Multi-Target Localization

MAHSA MOHAMMADI AND MICHAEL W. SHAFER
Department of Mechanical Engineering, Steve Sanghi College of Engineering, Northern Arizona University, Flagstaff, AZ 86011, USA
Corresponding author: Michael W. Shafer (Michael.Shafer@nau.edu)

This work was supported by the National Science Foundation (NSF) under Grant 2104570.

ABSTRACT Localization of radio-tagged wildlife is essential in environmental research and conservation. Recent advancements in Uncrewed Aerial Vehicles (UAVs) have expanded the potential for improving this process. However, a key challenge lies in the optimal choice of waypoints for UAVs to localize animals with high precision. This study addresses the intelligent selection of waypoints for UAVs assigned to localize multiple stationary Very High Frequency (VHF)-tagged wildlife simultaneously, with a primary emphasis on minimizing localization uncertainty in the shortest possible time. At each designated waypoint, the UAV obtains bearing measurements to tagged animals, considering the associated uncertainty. The algorithm then intelligently recommends subsequent locations that minimize predicted localization uncertainty while accounting for constraints related to mission time, keeping the UAV within signal range, and maintaining a suitable distance from targets to avoid disturbing the wildlife. The evaluation of the algorithm's performance includes comprehensive assessments, featuring the analysis of uncertainty reduction throughout the mission, comparison of estimated animal locations with ground truth data, and analysis of mission time using Monte Carlo simulations.

INDEX TERMS Decision making, localization, radio telemetry, path planning, UAV, uncrewed aerial vehicle, autonomous aerial vehicle, wildlife monitoring.

I. INTRODUCTION

The use of uncrewed aerial vehicles (UAVs) for wildlife localization has gained significant attention in recent years due to their ability to efficiently cover vast and inaccessible terrains. Recent studies have demonstrated their effectiveness in tracking various animal species, highlighting their potential to revolutionize conservation efforts. Additionally, UAVs can be employed for various tracking techniques, including thermal imaging, radio tracking, acoustic tracking, and direct visual observation, each providing unique insights into animal behaviors and movements [1], [2], [3], [4]. These methods have been successfully used to monitor a wide range of species, from large mammals to small species [2], [3], [4], [5]. Among these techniques, telemetry with very high frequency (VHF) tags has proven particularly effective for tracking smaller animals and those in dense habitats where GPS signals may be unreliable. Moreover, VHF is often used in combination with GPS for larger collar tags.

In recent years, several researchers have developed tracking systems to estimate the location of VHF transmitters with UAVs. There are two general approaches to the estimation problem: bearing-based and range-based. Bearing-based estimation refers to a method of estimating the location of an object based on the angles from which it is observed. The systems referenced in [6] and [7] have employed this approach. This estimation technique is mainly based on the direction of arrival (DOA), which refers to the angle at which a signal reaches a receiver relative to a reference direction (usually north). In this context, the UAV performs a 360° azimuthal scan, meaning it rotates in place to sweep through all possible directions on the horizontal plane, allowing it to receive signals from different directions. By measuring the strength of the pulses received at various angles, the UAV identifies the bearing to the target, which indicates the direction in which the target is located. Previous work [8]

The associate editor coordinating the review of this manuscript and approving it for publication was Akshay Kumar Saha.

employed this technique with an H-type directional antenna, which has been traditionally used in manual search methods by wildlife trackers.

In contrast, range-based estimation refers to a method of estimating the location of an object based on distance. Systems presented in [9], [10], and [11] are examples of this method. This localization method mainly uses Received Signal Strength Indicator (RSSI) as a metric to estimate the distance between the radio receiver and the radio transmitter. However, as demonstrated in [12], RSSI can be highly unreliable for distance measurement due to its susceptibility to environmental factors and inconsistent behavior, even under ideal conditions. These issues make range-based estimation less dependable for accurate localization in practice. Therefore, this paper adopts the bearing-based estimation approach for the UAV localization system. Regardless of which approach is used, Bayesian estimation is often used by many of these systems to accomplish the estimation problem. For example, particle filtering is used in systems presented in [9], [10], and [13].

The localization techniques discussed can greatly benefit from effective path planning strategies. Path planning is essential for UAV-based tracking systems, especially when surveying vast and remote terrains spanning several kilometers. Effective path planning enhances localization by guiding the UAV to optimal waypoints that improve measurement quality. Unlike static patterns, such as lawnmower paths–a back-and-forth motion used for full area coverage–, dynamic path planning allows the UAV to adapt to real-time data, prioritize high-value measurements, and respond to changing environmental conditions. For example, the ability to adjust to dynamic targets makes the localization process more responsive, allowing the UAV to update its waypoints in real time based on the movements of the targets. It can also minimize mission time by strategically optimizing the number and locations of the UAV's waypoints, which helps conserve battery life and reduce operational costs. Additionally, it helps avoid disturbing wildlife by maintaining safe distances while still collecting reliable data. Overall, with its ability to maximize resource utilization, improve scalability, and adapt to dynamic environments, path planning is essential for achieving precise, efficient, and ethical UAV-based wildlife tracking missions. Despite these numerous advantages of optimal waypoint selection, many systems designed for wildlife tracking have not addressed this aspect. For example, a system with a novel range-based estimation approach was presented in [14], however, they used a lawnmower pattern as the UAV's flight path, where the UAV travels up and down parallel lanes. Researchers in [15] who developed an aerial VHF tracking system using a novel multi-channel receiver also used the same pattern for the flight paths. The lawnmower pattern has also been used in [16], which designed a fully custom-built active RF identification tag and receiver system and presented a new and simple estimation approach based on mean coordinates. Path planning algorithms for autonomous systems have been proposed in the literature, but many have only been tested on ground-based or underwater systems. For instance, [17] examined an active localization strategy called Cautious Greedy Strategy, using an Extended Kalman Filter (EKF) for a mobile robot with a loop antenna.

In the context of UAVs, various methods have been proposed in recent studies. For instance, [18] described an approach that utilized Shannon entropy for path planning, while did not consider mission time optimization. Researchers in [11] employed Rényi divergence in their system for planning, but localizarion is range-based and prone to environmental effects. LAVAPilot, proposed in [19], aimed to reduce computational costs by using a task-based strategy but instead increased mission time. Another strategy to choose waypoints during execution was introduced in [20], aiming to reduce uncertainty at each step using bounded bearing measurements. However, this approach is limited to a single stationary target. The problem of online path planning for joint detection and tracking of multiple unknown radio-tagged objects, using a partially observable Markov decision process with a random finite set track-before-detect multi-object filter (RFS-POMDP), is considered in [21].

While these key advancements are noteworthy, several gaps remain unaddressed in current methodologies. Notably, some algorithms are designed to operate offline and fail to consider real-time constraints. Additionally, some are computationally intensive and yet need to be adapted for real-time online applications. Also, certain approaches do not factor in mission time optimization, which is crucial for practical battery limited operations. Furthermore, many existing solutions are designed to track only a single tag, limiting their applicability in real-world cases where multiple animals often need to be tracked simultaneously. This research aims to bridge these gaps by developing an online planning algorithm that minimizes localization uncertainty and mission time, enabling real-time tracking of multiple VHF-tagged animals.

In summary, the main contributions of this research are as follows: 1) A *novel online* method for path planning to track *multiple targets* that focuses on reducing *target position uncertainty*; 2) Optimization of *mission time*, which is crucial for energy-limited platforms such as UAVs; 3) Incorporating *battery energy constraints* into the planning process; 3) consideration of *potential signal loss* from targets to ensure robust tracking; and 5) maintenance of a *safe distance* from targets to minimize disturbances and errors.

This work illustrates the initial development of the algorithm, with future efforts focused on its advancements and testing it on a UAV in real-world situations.

II. MATERIALS AND METHODS

A. PROBLEM STATEMENT AND ALGORITHM OVERVIEW

The software and hardware required to implement the system are comprehensively detailed in previous work [8]. Building on this foundation, the proposed model focuses on the UAV's

operation, where it flies in a 2D horizontal plane at a constant altitude. This plane is discretized into a set of potential future waypoints, $R = \{r_1, \ldots, r_m\}$. As mentioned, the proposed approach employs bearing-based localization, where each waypoint provides bearing angles μ_i(for $i = 1 : n$) to n tags. To find bearings, the UAV rotates in place to change the direction of the mounted directional antenna, and this rotation is discretized into steps. At each step it receives pulses from transmitters. Using these pulses, the bearings to the targets can be estimated (Figure 1). A Principal Component Analysis (PCA)-based method is employed to estimate the bearing by leveraging all received pulses at a waypoint. PCA identifies the direction with the largest variance in the received signal data, determining the signal's direction relative to an earth-fixed reference frame. This process involves constructing a data matrix from the received pulse power and performing PCA to extract the primary direction of the signal. For a more detailed explanation of this approach, please refer to the previous work [8].

Factors such as multi-path effects can introduce errors in bearing measurements, resulting in uncertainty in each estimated bearing. The uncertainty associated with each bearing angle is modeled as a wedge-shaped region, referred to as an uncertainty wedge, which spans a constant angle α around each bearing line (Figures 1 and 2a). This wedge represents the possible range of error in the bearing measurement. Specifically, the algorithm assumes that the true bearing lies somewhere within the angular range from $-\frac{\alpha}{2}$ to $+\frac{\alpha}{2}$ relative to the measured bearing. The length of the wedge is the maximum reception range of the receiver. Given this model, the UAV requires $\frac{360}{\alpha}$ steps to complete each rotation for bearing estimate. This bounded uncertainty model has been employed in previous studies, such as in [13] and [20]. It is preferred over probabilistic models due to its computational efficiency, enabling faster real-time processing. At each waypoint, new bearings and associated wedges are introduced. Localization is achieved by iteratively intersecting these bearing wedges, resulting in refined regions of position uncertainty for each tag (Figure 2b). The targets are assumed to be located at the centroids of these intersections. The objective is to minimize the spread of these uncertainty regions around expected tags' locations (Figure 2b). To minimize the dispersion of position uncertainty, the concept of the second polar moment of area is utilized, which quantifies the distribution of area away from a central point. This approach was chosen over simply minimizing the area to simultaneously reduce the dispersion in both the X and Y directions. The second polar moment of area, J, is given by

$$J = \int \int_A r^2 \, dA \tag{1}$$

where A here represents the area of the uncertainty region and r is the distance from expected tag locations to a differential area element dA. This will be discussed in detail in section II-B.

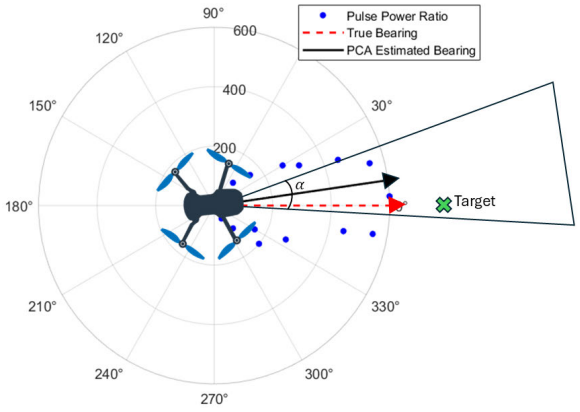

FIGURE 1. Obtaining bearings to targets using received pulses during an azimuthal scan. As the UAV rotates in place at each waypoint, it receives pulses from the target (blue dots). Using the PCA method, these pulses are used to estimate the bearing to the target (black arrow). The uncertainty for each estimated bearing is modeled as a wedge with an angle α, extending symmetrically around each bearing line. The algorithm assumes that the true bearing (red arrow) lies within this uncertainty wedge. PCA, principal component analysis.

Another key objective of the algorithm is to accelerate the mission. Accelerating the mission is critical because UAVs have limited battery life, which restricts their operational duration. Efficient use of time ensures that the UAV can complete its tasks within its power constraints. Hence, for each potential waypoint in R, two objective functions need to be calculated, making the optimization problem multi-objective in nature with the goals of minimizing the dispersion of uncertainty areas and time. To solve this problem, the Pareto front is employed to identify efficient choices for the next waypoint. Moreover, sufficient energy is allocated for each movement, guaranteeing an adequate number of waypoints. Additionally, when determining the next waypoint, the aim is to have at least one detectable tag within this range. This allows the UAV to be sent to locations where tag signals remain robust. Finally, the UAV is always kept at a distance from the target animals to avoid approaching them too closely. This precaution serves two purposes: first, to avoid compromised bearing estimates caused by the UAV flying directly above the tags, and second, to minimize disturbance to the animals' natural behavior. Interwaypoint movements do not observe this constraint, but inclusion may be considered in the future.

B. DISPERSION OF POSITION UNCERTAINTY

As mentioned above, upon reaching the initial waypoint, the UAV takes bearing measurements for all n-detectable tags, resulting in corresponding wedges of uncertainties around each bearing line. In this work, the first waypoint is assumed to be directly above the launch location, as no prior information about the targets' locations is available. However, if an initial estimate of the targets' locations is provided, the first waypoint can be selected based on this

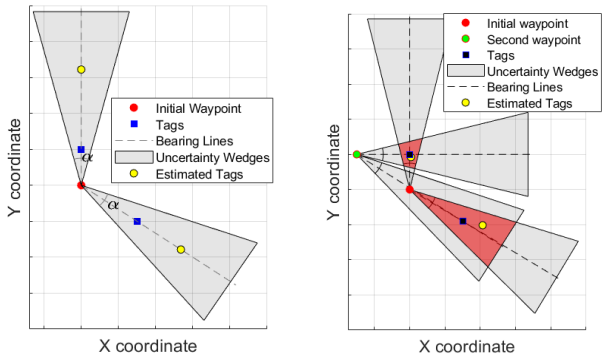

FIGURE 2. Uncertainty Model: (a) Initial bearing lines and corresponding uncertainty wedges at the first waypoint; (b) Refined uncertainty regions after the second measurement. One tag exhibits a small dispersion of uncertainty indicating higher localization precision, while the other tag shows a larger dispersion area, reflecting greater localization error. The goal is to reduce the spread of these position uncertainties for all of the tags simultaneously, by optimally selecting the best future waypoint.

information. The challenge lies in determining where to travel next to ensure that the resulting intersection area–between the previous position uncertainty and the new wedge of uncertainty–is minimized in terms of dispersion, for all tags. Within each uncertainty area, there is a set of points $P = \{p_1, \ldots, p_k\}$, representing the candidate tag locations for the specific target. For each r_j in R, the dispersion of uncertainty around the candidate tag p_s is calculated, if we were to select this point as next waypoint, and subsequently received a bearing at r_j to p_s. This area results from the intersection of the current uncertainty area and the *expected* uncertainty wedge, assuming the point p_s in P represents the tag and r_j is the next waypoint. The resulting second polar moment of area is denoted as $j(r_j, p_s)$. These values are then summed across all candidate tag locations for tag i as

$$j_i(r_j) = \sum_{s=1}^{k} j(r_j, p_s). \tag{2}$$

This process is illustrated in Figures 3a and 3b. In this example, two potential future waypoints r_1 and r_2 are shown, with two potential tag locations p_1 and p_2 inside the uncertainty wedge after the first measurement. The total second moment of area for r_j associated with tag i will be $j_i(r_j) = j(r_j, p_1) + j(r_j, p_2)$. Note that this is for illustration only. There are typically many candidate tag positions within the uncertainty areas depending on the size and discretization used. As it is shown in Figure 3b, $J_i(r_2)$ would be optimal choice in this case, producing smaller dispersion for expected intersections.

If there is more than one tag, the results for all n tags are summed. Dynamically adjusting weights (w_i) and then using weighted sum could be employed depending on the remaining uncertainty for each tag, as shown in 3. However, uniform weighting was employed in this study ($w_i = 1, , i = 1 : n$).

$$J_1(r_j) = \sum_{i=1}^{n} w_i j_i(r_j). \tag{3}$$

In this way, the first objective function is established for all the points in R. Figure 4 demonstrates a J_1 example contour. In this scenario, there is one tag, and the UAV is at the first waypoint. The results are logical: points near the uncertainty wedge and those leading to a perpendicular bearing relative to the previous bearing have lower J_1 values, indicating they will result in reduced uncertainty dispersion. The excluded locations in this example (white area) are those that are potentially above the target.

C. TIME

The next objective function calculated for potential future waypoints is time. This objective function includes the sum of the measurement time at a given waypoint and the travel time required to reach that point from the current waypoint. Leveraging the assumption of constant translational velocity, it is formulated as

$$J_2(r_j) = \frac{|r_{\text{UAV}} - r_j|}{V_h} + t_{\text{measurement}}. \tag{4}$$

Here, r_{UAV} represents the current coordinates of the UAV, V_h is the horizontal velocity of the UAV, and $t_{measurement}$ is the time required to take the measurement at the given waypoint, which equals to the number of steps when the UAV is performing azimuthal scanning ($\frac{360}{\alpha}$) multiplied by the time taken at each of these steps.

D. REFINING CANDIDATE WAYPOINTS

In the algorithm, before formulating the objective functions at each step, the list of locations for the UAV in R must be refined based on the constraints. The following categories of points must be excluded:

1) POINTS THAT THE UAV DOES NOT HAVE SUFFICIENT ENERGY TO REACH

An energy model was developed to govern the UAV's movement between two points in three-dimensional space. While the localization model operates with the UAV flying in a 2D horizontal plane at a constant altitude, the energy model also accounts for the third dimension, z, when modeling the energy required for vertical transitions. The inclusion of the vertical dimension is limited to energy considerations related to takeoff and landing, as the UAV's movement in all other aspects remains confined to the 2D plane as previously discussed. The energy model serves the purpose of ensuring sufficient energy allocation for each UAV movement to maintain desired number of waypoints, but could be updated in the future to use real-time power measurements from the vehicle.

In steady-state flight, the thrust vector of the UAV can be divided into three primary components: the force to overcome gravity, the force to climb, and the force to overcome

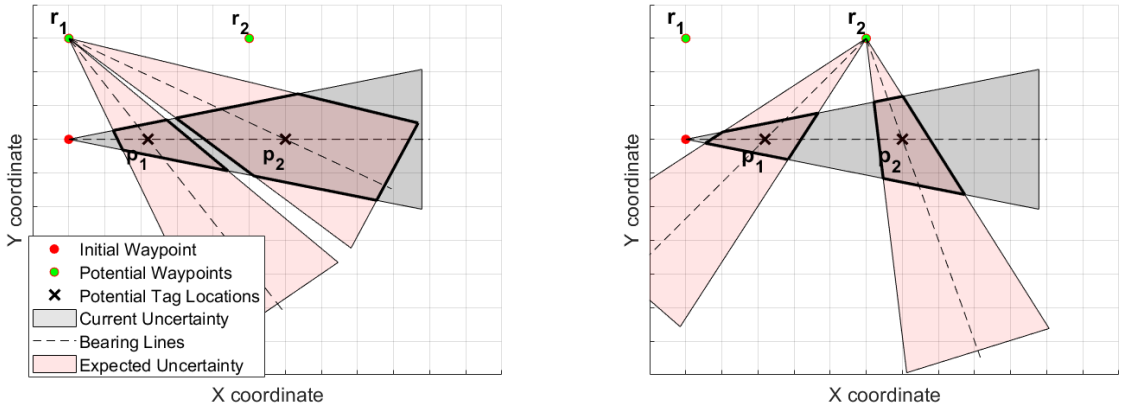

FIGURE 3. Calculation of the First Objective Function J_1. The current uncertainty after the initial measurement is shown by the gray wedge. r_1 and r_2 are potential next waypoints. (a) Selecting r_1 results in the expected uncertainty areas shown by the pink wedges. The intersections exhibit large dispersion, demonstrating greater uncertainty. (b) Selecting r_2 leads to the expected uncertainty areas with smaller dispersion, suggesting a better choice compared to r_1.

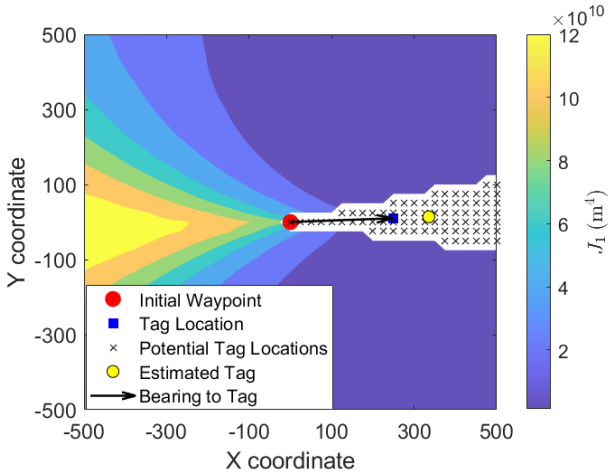

FIGURE 4. One example of a contour plot of J_1. The color gradient illustrate the values of J_1, with lower values indicating smaller predicted uncertainty dispersion after the next measurement.

translational drag. Instead of integrating these forces over the distance between two points in space, the power required by each component is superimposed, and this power is integrated over time to estimate the energy expended. The energy required to overcome gravity, translate, and climb is now discussed.

Gravity: The power to hover is assumed to be equal to the energy capacity of the battery, E_{batt}, divided by the maximum hover time measured in testing, t_{hover}. This relationship is expressed as $P_{hover} = E_{batt}/t_{hover}$. This accounts for all electrical and aerodynamic inefficiencies of the propulsion system. Neglecting transients during movement, the energy is simply the time integral of this constant power

$$E_{hover} = P_{hover}\,\Delta t. \tag{5}$$

Climb/Descent: The additional energy to move between two vertical points can be assumed to be equal to change in potential energy. Aerodynamic drag is neglected during climb, assuming the energy required for climb is much greater than that lost to aerodynamic drag. Also, even though the perturbation to the thrust force may generate some additional aerodynamic or electrical inefficiencies, these deviations from those accounted for within the gravity/hover term are assumed to be negligible. If these are determined in future testing to be non-negligible, a simple efficiency terms η_c or η_d can be incorporated into the following energy terms as shown

$$E_{climb/descent} = mgz(\eta_c H(z) - \eta_d H(-z)) \tag{6}$$

where z is the vertical distance, and H(z) represents the Heaviside function.

Translation: A bluff body aerodynamic model is assumed for translational force, such that the drag force can be modeled as $F_d = \frac{1}{2}\rho C_d A_x V_h^2$, where ρ is the atmospheric density, C_d is the coefficient of drag, A_x is the cross sectional area of the vehicle in the vertical plane, and h is the horizontal distance between points. The coefficient of drag is unknown, but will likely be in the range $1 < C_d < 1.3$ as a cube has a value of 1 and the addition of the arms and landing gear will push this value above 1. The power to overcome this drag force is thus $P_{translate} = \frac{1}{2}\rho C_d A_x V_h^3$. Once again assuming steady state flight, the energy beyond that is required for hover would be

$$E_{translate} = \frac{1}{2}\rho C_d A_x V_h^3 \Delta t. \tag{7}$$

In (5) and (7), Δt is defined as $\Delta t = max(\Delta t_z, \Delta t_h)$, where $\Delta t_z = \frac{z}{V_{z-max}}$ and $\Delta t_h = \frac{h}{V_{h-max}}$. Finally, total energy to travel from point A to point B is the sum of the three energy terms as expressed below

$$E_{total} = E_{hover} + E_{translate} + E_{climb} \tag{8}$$

To ensure adequate energy allocation for each UAV's travel, the energy required to navigate the UAV from the launch location to the first waypoint is first computed, along with the energy needed for the initial measurement at that waypoint. Furthermore, a portion of the UAV's total energy capacity is reserved to guarantee a safe return to the launch location. This reserved energy could be the energy needed to return from the furthest location to the launch site. Next, this cumulative energy is subtracted from the total battery energy. The remaining energy is then evenly divided into equal segments, representing the allocation for subsequent travels. When selecting the next waypoint, destinations requiring more energy than the allocated portion for travel are systematically excluded.

2) POINTS THAT MAY CAUSE SIGNAL LOSS

The next set of points to be excluded are those where flying to them might result in the loss of signals from all n tags. To prevent this, regions are identified for each tag where signal loss would occur if the UAV flies there, using the most recent estimates of tag locations. These are the locations that are beyond the expected maximum reception range (MRR) of the antenna. MRR values would be set based on user experience with tags and terrain interactions. For each tag, the points that cannot receive a signal are determined by the following equation:

$$|r_{tag_i} - r_j| > \text{MRR} \tag{9}$$

From these sets of points, the common points for all tags are identified. These common points must be excluded.

3) POINTS THAT MIGHT BE RIGHT ABOVE TARGETS

In addition to the previously identified exclusion zones, it is crucial to ensure that the UAV maintains a safe distance from the target animals to avoid inaccuracies in bearing estimates. Flying directly over the tags can compromise the antenna's directionality due to the diminished effectiveness of the 3D radiation pattern at low elevation angles. This approach also minimizes disturbances to the animals. For each tag, points within R that are closer to the potential tag locations than a defined threshold distance are excluded.

E. DECISION MAKING

With J_1 and J_2, each is normalized to the range [0, 1]. Using these normalized values, the Pareto front approach is employed to solve the multi-objective problem. The Pareto front helps to identify the set of non-dominated solutions,also known as the Pareto-optimal set, where no other solution is superior in both objectives. The algorithm computes the Pareto-optimal set by evaluating all potential waypoints and comparing the corresponding objective values, normalized J_1 and normalized J_2. Waypoints that are dominated–meaning there exist other waypoints that are better in at least one objective without being worse in the other–are excluded from the Pareto front. The remaining non-dominated waypoints form the Pareto-optimal set, which offers a range of options balancing uncertainty reduction and travel time. This concept is illustrated in Figure 9, which will be explained in more detail later in the paper. For more details on the Pareto front algorithm, see [22]. From this set of Pareto-optimal waypoints, different selections can be made depending on the optimization method or user preferences. In our case, the option that most effectively minimizes uncertainty is selected, as uncertainty reduction is currently prioritized over time minimization.

However, alternative methods can be used when choosing the optimal choice. For instance, there are cases where the best point for uncertainty reduction and another point on the Pareto frontier are not significantly different in terms of minimizing uncertainty (less than $\delta_{\text{normalized } J_1}$), but vary greatly in terms of travel time (more than $\delta_{\text{normalized } J_2}$). Here, $\delta_{\text{normalized } J_1}$ represents a small, acceptable threshold for the difference in uncertainty reduction, and $\delta_{\text{normalized } J_2}$ refers to a threshold for differences in travel time. In these cases, the point with shorter travel time can be chosen. This ensures that minimal gains in uncertainty reduction are not prioritized at the cost of significantly increased travel time. Both selection approaches have been tested, and the results are compared in Section III.

Algorithm 1 outlines the step-by-step process of the multi-objective UAV path planning algorithm, which is also illustrated in the block diagram shown in Figure 5.

III. SIMULATION

A. SIMULATION SETTINGS AND RESULTS

To validate the performance of the proposed planning and localization algorithm, 1000 iterations of Monte Carlo simulations were conducted. Each iteration involved randomly generated 3 tag locations from a uniform distribution, within a 1 km $\times$ 1 km region, with the UAV operating at a constant altitude of 100 m. The mean and standard deviation of the initial distances between the UAV and the tags have been reported in table 1. The UAV used in this simulation has a mass of 5 kg and a battery capacity of 16,000 mAh with a voltage of 14.8 V. It has a maximum climb speed of 3 m/s and a maximum horizontal velocity of 15 m/s, with a cross-sectional area of 0.2 m $\times$ 0.2 m. To ensure the mission's feasibility, enough energy is reserved for the UAV to return from the farthest point in its flight plane, $\sqrt{1\,\text{km}^2 + 1\,\text{km}^2}/2$, back to the launch location at $(0, 0)$ on the ground, using (6) and (7). The UAV must complete its mission, including travel and measurements, within the remaining battery capacity. Throughout the mission, the UAV visits four distinct waypoints. Each bearing measurement is associated with an uncertainty wedge with $\alpha = 20°$. The rationale for selecting these values will be discussed later. The resolutions for points in R and P were set to 25 m. The simulation begins with the UAV at the origin, where it initializes bearing measurements for all three tags. During this process, points in R within 50 m of the potential tag locations were excluded. However, due to the sufficient battery capacity, no additional points were excluded based

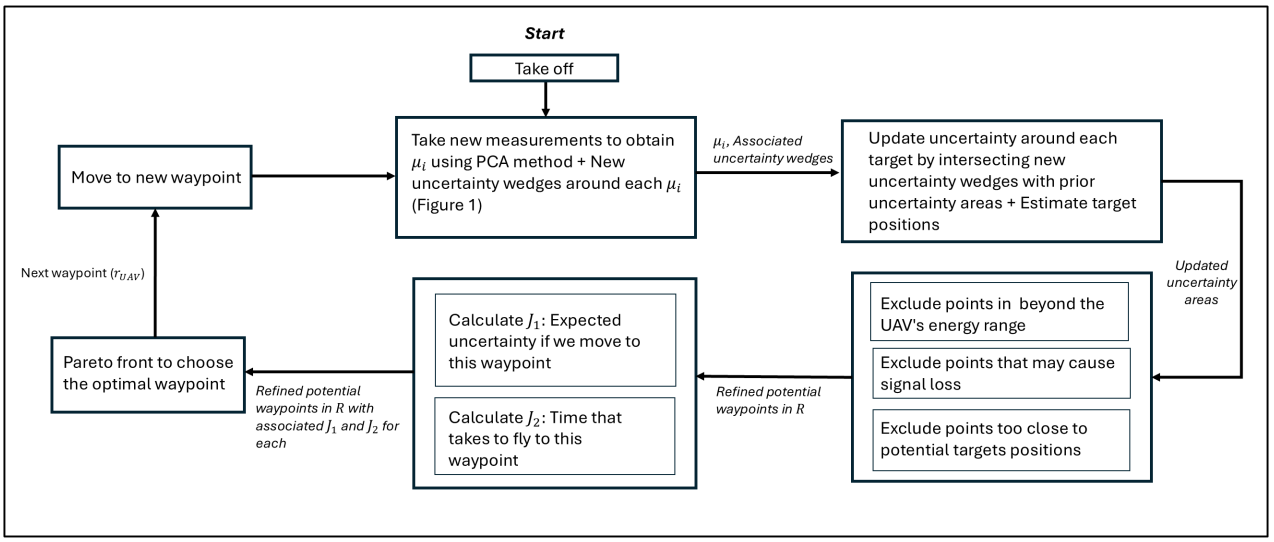

FIGURE 5. Block diagram of the UAV Path Planning Algorithm. This diagram illustrates the main components of the algorithm and the flow of data.

on energy constraints. Additionally, the maximum reception range for the antenna to detect signals from the tags was set to 3 km. Since all tag locations within the region were within the reception range of the UAV's antenna, no points were excluded due to potential signal loss. Future work will investigate the effect of these constraints.

The performance of the algorithm was evaluated using three key metrics: reduction in uncertainty area, localization error, and mission time. The reduction in uncertainty area measures the total decrease in the area where the tag could be located, with larger reductions indicating higher precision. Localization error represents the distance between the actual and estimated tag positions, with smaller errors indicating greater accuracy. Mission time refers to the total duration of the UAV's mission, including travel and measurement times, with shorter times preferred for efficiency.

Two sets of simulations were conducted. In the first set, no bearing error was assumed. In the second set, bearing errors were incorporated, modeled using the von Mises circular distribution $\mathcal{V}(\mu, \kappa)$. The mean μ was set to zero for the von Mises distribution parameters. Based on previous work [8], the standard deviation of the bearing error, determined through testing, was chosen to be 6.7 degrees. Using the equation below (see [23])

$$\kappa = \frac{1}{\sigma^2} \tag{10}$$

where σ represents the standard deviation, the concentration parameter κ was calculated to be 73. The results have been shown in Table 1.

In these simulations, waypoint selection prioritizes the point offering the greatest uncertainty reduction from the Pareto front, as discussed. However, an alternative method was also explored by adjusting the selection criteria. Specifically, if the difference in uncertainty reduction between a point and the one that minimizes uncertainty is small (set to less than 5%), but the difference in travel time is significant (set to greater than 20%), the point that requires less time to reach is selected. The comparison of results from both methods is presented in Figure 6. This approach results in an average reduction of approximately 10% in travel time, while compromising less than 1% in uncertainty reduction and resulting in negligible changes in localization error. Notably, the localization error is sometimes lower with this method, which can be attributed to the shape of the final uncertainty region, as the centroid is used as the estimate for tag locations. Based on these results, this method may be considered for adoption over the current one in future real-world testing.

To illustrate the process, an example is presented in Figure 7, using the first method of waypoint selection. In this example, three tags are located at $(400, -200)$, $(400, 200)$, and $(-50, 400)$. The initial uncertainty and associated potential tag positions are shown in Figure 7a. As expected, the initial estimates of tag locations are not accurate after the first measurement, but it converges over time. The suggested waypoints from the Pareto front are indicated by red crosses, representing points optimized for time (those near the UAV's current location) and uncertainty reduction. As mentioned earlier, the optimal point in terms of uncertainty reduction is selected from this set of optimal choices. Figure 9 shows the Pareto front for selecting the second waypoint. After the second measurement, shown in Figure 7b, the uncertainty decreases, and the tag position estimates improve. This improvement continues in the third step, as shown in Figure 7c. The final state after the fourth measurement is shown in Figure 7d. Although the process could continue, based on the analysis for localization of three tags, further measurements would result in very small reductions in uncertainty, making it optimal to stop here.

TABLE 1. Summary of monte carlo simulation results.

Metric	No Bearing Error		With Bearing Error	
	Mean	Std	Mean	Std
Uncertainty Reduction (%)	99.15	0.54	99.49	0.33
Mission Time (s)	263.67	25.23	259.52	25.68
Localization Error (m)	13.33	5.53	40.20	19.01
Average Waypoint Computation Time (s)	12.36	2.16	12.84	2.57
Average Initial Distance from UAV to Targets (m)	379.83	83.64	379.83	83.64

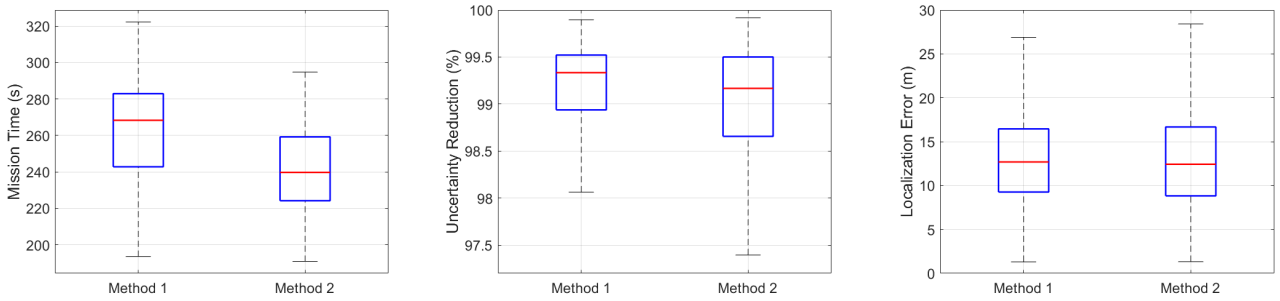

(a) (b) (c)

FIGURE 6. Comparison of uncertainty reduction, travel time and localization error between two waypoint selection methods: Method 1: Selectinglocation with greatest uncertainty reduction on Pareto frontier. Method 2: Location with shorter travel time is selected when the improvement inuncertainty reduction is marginal (less than 5%) and the difference in travel time is substantial (greater than 20%).

However, if more tags were present, additional waypoints might be necessary. It is important to note that if, due to errors in the bearing estimate, the new bearing is significantly inaccurate and no intersection is obtained, prior information is relied upon instead. Figure 8 displays the second method of waypoint selection for this case. In this case, the alternative method reduced mission time by 34% while increasing average uncertainty by less than 1%. The optimization process for selecting the second waypoint using both methods in this example case is illustrated in Figure 9.

B. SIMULATION VARIABLES

The performance of the algorithm is influenced by various factors. Firstly, the effect of the size of the uncertainty wedge was investigated by testing different values for α to determine how varying levels of measurement uncertainty influenced the algorithm's results. Secondly, the impact of the number of tags on performance was examined by varying the number of tags from 1 to 3 within the simulation region. Additionally, the variation of localization error and uncertainty as functions of the waypoints was investigated. Lastly, the effect of different discretization levels of R on the algorithm's performance was evaluated.

The analysis of wedge size, as shown in Table 2 and Figure 10 indicates that as the wedge size increases, the remaining area of uncertainty around each tag, as well as localization error also increase. This outcome is expected, as larger wedges imply greater measurement uncertainty. However, the mission time decreases with larger wedge sizes because the UAV spends less time at each waypoint due to the shorter measurement time required. This is because, as mentioned, the number of steps is $\frac{360}{\alpha}$; hence, larger α results in fewer steps per rotation. These results suggest that there is an optimal wedge angle α that balances effective localization with minimal mission time. Based on the analysis, $\alpha = 20°$ was selected for this region area, as this value provides a trade-off between localization accuracy and mission efficiency.

TABLE 2. Mission time and uncertainty reduction for different α values.

α(degree)	Time (s)		Uncertainty Reduction (%)	
	Mean	Std	Mean	Std
16	302.87	25.87	99.53	0.28
20	234.45	24.46	98.70	0.78
24	180.48	20.51	97.08	1.37
36	155.51	17.89	95.67	1.72
90	70.33	18.15	79.47	3.68

As demonstrated in Table 3, the analysis of the effect of the number of tags shows that increasing the number of tags, while keeping the same number of waypoints, leads to a larger final area of uncertainty around each tag. This occurs because, with fewer tags, the UAV can utilize the waypoints more effectively to closely approach each tag, thereby reducing the uncertainty. However, as the number of tags increases, the UAV's waypoints must be distributed among more tags, providing fewer opportunities to sufficiently reduce the uncertainty around each individual

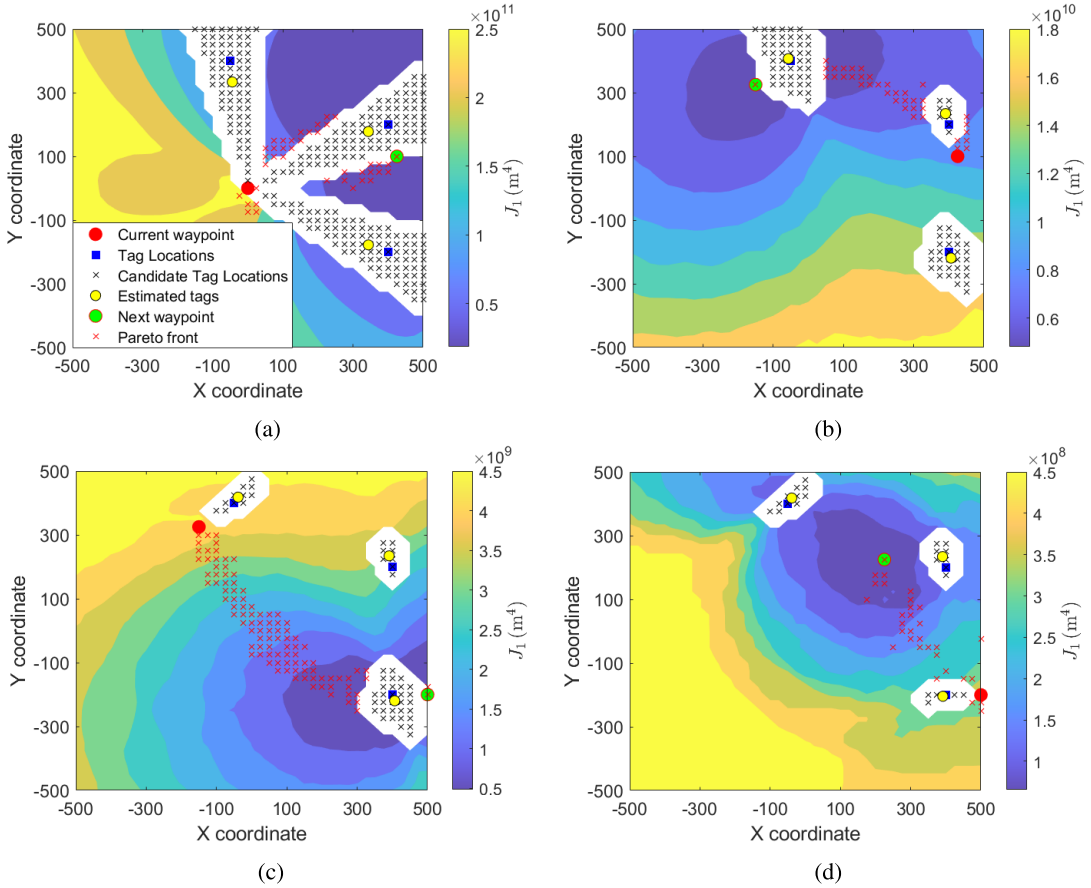

FIGURE 7. Waypoint selection for localization of three tags: (a) shows the first step, where UAV starts the mission from the origin. white regions are the areas that cannot be selected as the next waypoint. The localization error is substantial. (b) After second measurement the localization has been improved. (c) After the third measurement (d) The final state.

tag. Similarly, the localization error tends to increase with the number of tags, reflecting the difficulty in accurately estimating the positions of a larger set of tags within the same operational constraints (Figure 11). Consequently, more waypoints are likely needed to achieve the same level of uncertainty reduction as with fewer tags. Nonetheless, in our tests, four waypoints appear to be sufficient for the given number of tags, as the results show only slight differences in terms of uncertainty reduction and localization error. Mission time tends to increase as the number of tags increases. This is because, with more tags, the UAV often needs to cover greater distances between targets, leading to longer mission times.

To analyze the impact of the number of waypoints on localization performance, Figure 12 illustrates the variation of uncertainty regions and localization error across waypoints. Results from scenarios without bearing error are compared (Figures 12a and 12b) with those including bearing errors (Figures 12c and 12d). The results indicate a significant improvement in both parameters from the first to the second waypoint. However, beyond the second waypoint, this rate of improvement diminishes. The number of waypoints ultimately depends on user preference and represents a trade-off between mission efficiency and localization accuracy and precision. As discussed, for the scenario involving three targets, four waypoints appear to be sufficient, as the changes observed at the fifth waypoint are minimal.

TABLE 3. Mission time and uncertainty reduction for different numbers of targets.

Number of Tags	Time (s)		Uncertainty Reduction (%)	
	Mean	Std	Mean	Std
1	205.23	6.3	99.88	0.05
2	245.26	27.9	99.4	0.55
3	263.68	25.4	99.15	0.54

Regarding the discretization level of R, finer discretization increases the resolution of potential waypoint selection, allowing for a more comprehensive exploration of the solution. This higher resolution improves the likelihood of identifying the optimal waypoint for minimizing both objective functions. However, this improvement comes with the trade-off of increased computational complexity, as the optimization process must evaluate a greater number of potential waypoints. Therefore, selecting the resolution requires consideration to strike a balance between computational efficiency and algorithmic performance. However, as shown in the Table 4, for the region we tested, resolutions

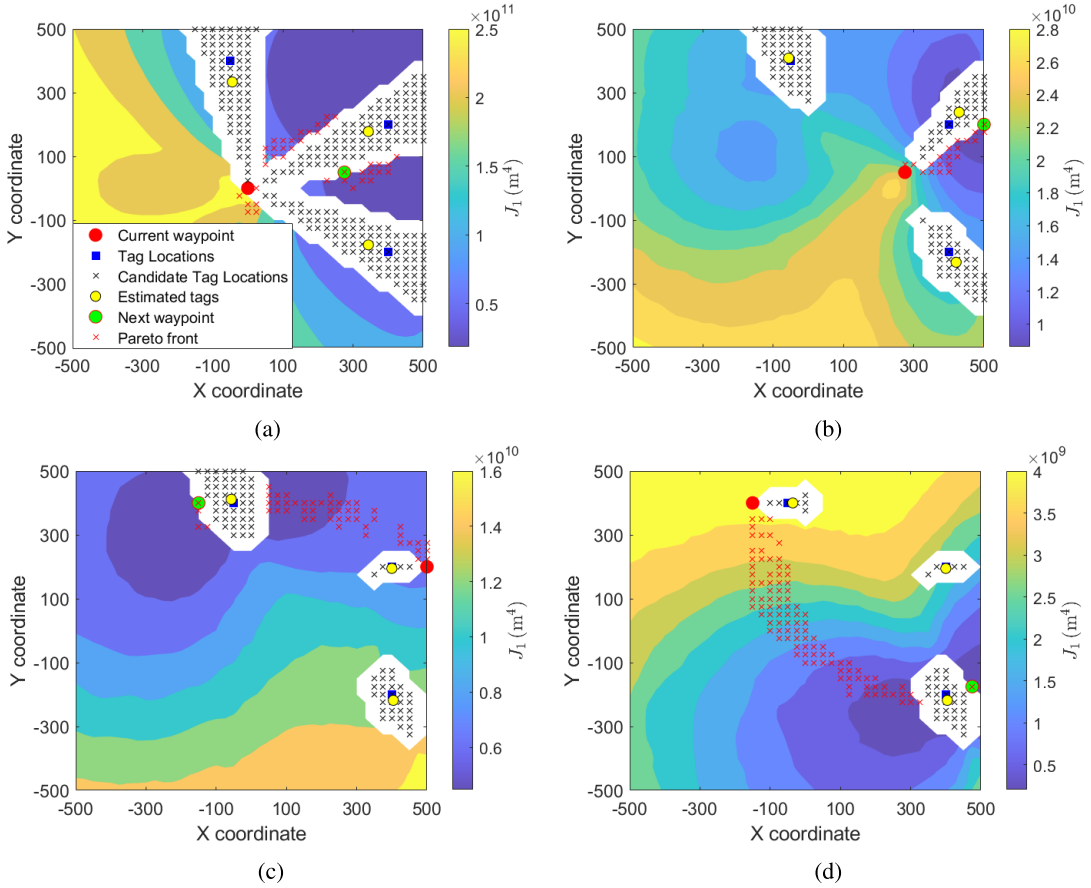

FIGURE 8. Waypoint selection process for the case shown in Figure 7, using the alternative method. In this approach, the criteria prioritize shorter travel time when the improvement in uncertainty reduction is small.

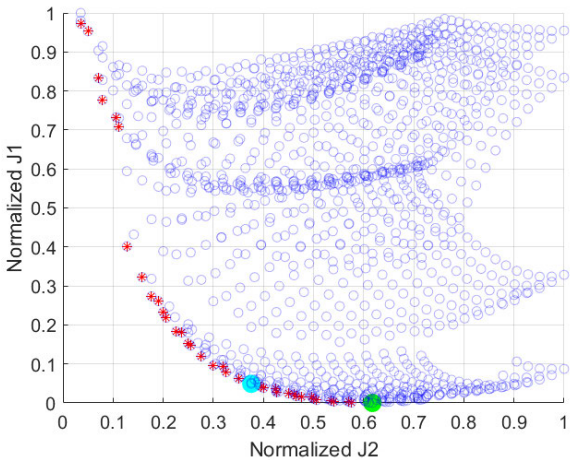

FIGURE 9. Pareto front of the optimization process for selecting the second waypoint in the case presented in Figures 7 and 8. The optimal solutions are represented by the red asterisks. The green circle indicates the point that has minimum uncertainty between optimal choices. The blue circle highlights the solution based on the alternative method, which balances travel time and uncertainty reduction.

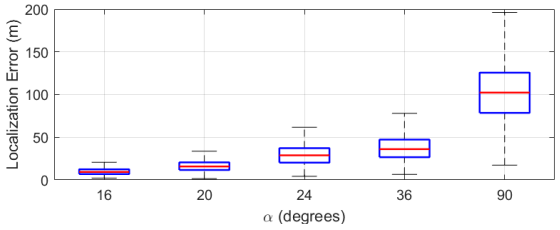

FIGURE 10. Effect of wedge size on localization error.

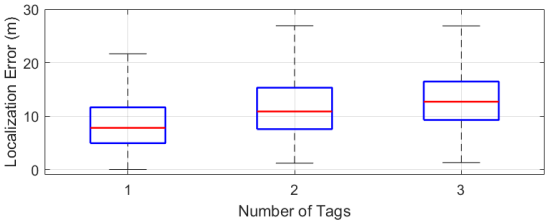

FIGURE 11. Effect of the number of tags on localization error.

of 15, 25, and 35 m showed no significant change in the performance of the algorithm. Based on the results, a resolution of 25 m was selected for our tests as it yielded the lowest localization error while maintaining an acceptable computation time.; however, opting for 35 m could have further reduced computation time.

Algorithm 1 UAV Path Planning Algorithm

INITIALIZE: R, r_{UAV}
Measure initial bearing angles μ_i for all tags
Initialize uncertainty wedges for each tag
for iteration = 1 to number of waypoints -1 **do**
  Refine potential locations:
  for each r_j in R **do**
    if energy required $>$ available energy **then**
      Exclude r_j from R
    end if
    Calculate the distance to each potential tag position
    if distance $<$ threshold distance **then**
      Exclude r_j from R
    end if
    Calculate the distance to each estimated tag position
    if distance $>$ maximum reception range for all tags **then**
      Exclude r_j from R
    end if
  end for
  Evaluate objective functions:
  for each remaining location in R **do**
    Calculate the dispersion of position uncertainty J_1 using (3)
    Calculate the second objective function J_2 using (4)
  end for
  Select optimal location:
  Identify the Pareto front of solutions for the trade-offs between J_1 and J_2
  Choose the location that minimizes J_1 from the Pareto front
  Move UAV to selected location and update r_{UAV}
  Take new measurements:
  take new bearing measurements μ_i for all tags
  Update uncertainty wedges and intersect with previous uncertainties
end for
End

TABLE 4. Localization error and mission time for different resolutions of R.

Resolutions	Localization Error (m)		Avg. Waypoint Computation Time (s)	
	Mean	Std	Mean	Std
15	14.39	6.15	33.16	5.24
25	13.33	5.53	12.84	2.57
35	13.59	5.59	6.33	1.28

IV. PERFORMANCE EVALUATION AND DISCUSSION

A. PERFORMANCE METRICS EVALUATION

As demonstrated in the previous section, the algorithm shows promising results in both localization accuracy and mission efficiency. The Monte Carlo simulation results for the case that considers error, summarized in Table 1, indicate that the approach achieves a mean uncertainty reduction of 99.49%

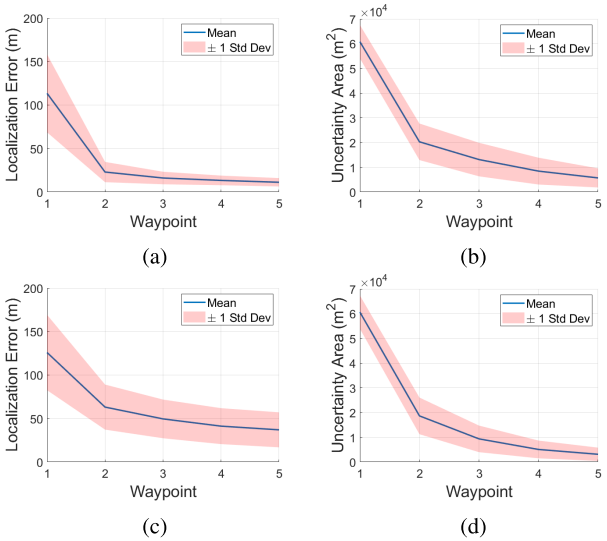

FIGURE 12. Changes in localization error and uncertainty regions across waypoints. (a) and (b) show the results for tests without bearing error. (c) and (d) present the results for tests with bearing error incorporated.

when localizing three tags with only four waypoints. The localization error achieved in this study is reasonable, with a mean value of 40.20 m, making it competitive with results from similar studies. Also, when comparing the results of the case with bearing error to the case without error, the uncertainty reduction remains almost unchanged. However, as expected, a higher localization error is observed, indicating strong precision despite lower accuracy.

It is important to note that the acceptable localization error in wildlife tracking depends on the application and study objectives, varying significantly based on the required precision and scale [24]. For example, for fine-scale behavioral studies, such as monitoring habitat use or social interactions, high accuracy is crucial to capture detailed movements [25], [26]. In home range and movement studies, moderate precision is sufficient to identify broader patterns. For population density and distribution assessments, even larger errors are acceptable as the focus shifts to identifying trends across expansive areas. Long-distance migration studies, such as tracking birds or whales, prioritize mapping migration routes over pinpoint accuracy [24]. Overall, the acceptable error reflects a balance between the study's goals, technological constraints, and the scale of the research. Based on these considerations, the localization error achieved in this study is acceptable for a wide range of wildlife tracking studies, from population density assessments to long-distance migration monitoring.

The mean mission time, excluding computation time for planning, was 259.52 s, indicating that the algorithm efficiently completes localization tasks within a reasonable timeframe. This duration depends on the number of waypoints and the number of tags being localized. Although this performance is entirely acceptable and significantly faster than a human tracker, as explained in Section III, it can be

further improved using the alternative method. This method, discussed earlier, resulted in an average 10% reduction in travel time with minimal impact on uncertainty reduction and localization error.

The average computation time was 12.84 s per waypoint, measured on a 13th Gen Intel(R) Core(TM) i7-1360P CPU running at 2.20 GHz with 16.0 GB of RAM. Given the total mission time of 259.52 s, the planning time is sufficiently low to ensure efficient mission execution. Additionally, as discussed in Section III-B, the computation time can be further reduced by selecting a coarser resolution for R, without degrading localization quality. It is important to note that this algorithm is intended for deployment on the ground control station's computer, where the specifications may vary, potentially affecting the computation time. While faster algorithms exist in the literature, such as [19], this duration remains satisfactory and suitable for online UAV applications.

B. COMPARISON

To highlight the performance and distinct advantages of the proposed algorithm, comparisons are made across three key benchmarks: a human tracker, a case without path planning, and existing path-planning methods.

Comparison with a human tracker: To evaluate the performance of the proposed algorithm, the results were compared with data gathered from a human tracker in previous work [8]. As shown in Table 5, a human tracker with over 20 years of experience achieved a localization error of 72 m when tracking a single stationary target, using six measurement locations aligned in a straight line at a distance of 500-570 m from the target. The mission time for the human tracker was calculated based on the time spent at each measurement locations (1 minute) and an average walking speed of 1.3 m/s. Covering a range of 140 m to complete six measurements took approximately 465 s. In comparison, the proposed system demonstrated significantly superior performance. As previously reported, it tracked three targets within a similar region in a much shorter mission time, requiring nearly half the time taken by the human tracker. Furthermore, the system achieved a substantially lower localization error compared to the human tracker, despite operating with a comparable bearing error. These results clearly highlight the superior performance of the algorithm compared to the human tracker in both mission time and localization accuracy.

Comparison with a Case without Path Planning: Results from the previous study, shown in Table 5, highlight the performance of the system without optimal waypoint selection. In this case, 12 waypoints arranged in a half-circle were used to localize a single stationary target, resulting in a localization error of 58 m. In contrast, the proposed system, which utilizes only four waypoints to track three targets, demonstrates not only a reduced mission times but also lower localization error.

Comparison with Existing Path Planning Methods: While several path-planning methods have been proposed in the literature for similar context, a direct comparison of results is challenging due to variations in experimental setups, such as the size of the test field, the initial distance from UAV to targets, or differing parameters used in each method. To address these differences, the proposed approach is compared with existing methods based on their algorithmic components and the features they incorporate. This comparison highlights the unique aspects of our method, such as its ability to handle multi-target tracking, minimize mission time, account for energy constraints, and address potential signal loss–all of which are critical for real-world applications. Table 6 presents a comparison of these aspects.

C. ASSUMPTIONS AND LIMITATIONS

One of the assumptions in this work is that the targets are considered stationary. This assumption simplifies the model and is often valid for specific scenarios, such as when animals are localized while asleep or exhibit minimal motion based on ecological data. Moreover, the significantly reduced mission time achieved by the UAV's optimal waypoint selection reduces the likelihood of animals moving during the localization process, further enhancing the feasibility of the stationary-target assumption in many practical scenarios. However, this assumption may not be suitable for all wildlife tracking applications. To extend the model for moving animals, future work could incorporate the estimated speed of the animals and calculate the maximum distance they could move during the UAV's travel to the next waypoint. For example, for animals with minimal to medium speeds this approach would remain effective. The α value can be adjusted to ensure the targets remain within the assumed area of uncertainty, maintaining the reliability of the localization process. Additionally, incorporating existing animal movement models [27] can be considered in future work to estimate potential target positions during waypoint planning.

Another assumption in this work is the absence of environmental factors such as signal interference and terrain effects. While we have accounted for bearing measurement errors to simulate some of these effects, real-world scenarios often involve more complex variations in signal propagation across different environments. Including detailed propagation models in future work would enhance the simulation framework, enabling it to better reflect real-world conditions.

Finally, regarding UAV movement, although the simulations in this study were conducted in a 2D environment, real-world wildlife habitats often feature complex 3D terrains that can influence the UAV's trajectory and sensing capabilities. Although operating the UAV at a sufficiently high altitude allows the proposed model to be applied in diverse terrains by minimizing the effects of elevation changes, this approach may not fully capture the challenges posed by complex 3D environments. Extending the simulation framework to

TABLE 5. Comparison of localization performance between the case with path planning, with predefined waypoints and a human tracker.

Method	Number of Waypoints	Bearing Errors Std (degree)	Mission Time (s)	Localization Error (m)
With Path Planning	4	6.7	260	40.20
Human Tracker	6	6.3	470	72
No Path Planning	12	6.7	824	58

TABLE 6. Comparison of algorithmic features across studies.

Study	Online	Energy Aware	Multi Target	Mission Time Consideration	Distance to Targets	Signal Loss Consideration	Targets' Movements
This Study	✓	✓	✓	✓	✓	✓	
Study [6]	✓						
Study [18]	✓		✓				
Study [20]	✓						
Study [11]	✓		✓				✓
Study [19]	✓		✓		✓		✓

account for 3D terrain features would provide a more comprehensive evaluation of the algorithm's applicability and robustness in real-world scenarios.

D. POTENTIAL APPLICATIONS AND FUTURE EXTENSIONS

The proposed UAV-based localization system has numerous potential applications across diverse fields besides wildlife tracking [28]. In search and rescue operations, UAVs can rapidly locate distress signals from emergency beacons or mobile devices in situations such as individuals lost in remote mountains or trapped after natural disasters in disaster zones [29]. In surveillance and security, UAVs can detect and track unauthorized transmitters, ensuring border security or monitoring critical infrastructure for unauthorized activities [30]. Also, an interesting extension of this work involves deploying a multi-UAV system, which could expedite the localization process and improve accuracy by leveraging multiple perspectives. The use of multi-UAV systems has been extensively explored in various fields, such as in [31]. Even though coordinating multiple UAVs poses challenges for wildlife tracking, as it introduces control complexities and increases risks of disturbing the animals, such systems could provide faster and more reliable localization when carefully managed.

V. CONCLUSION

This work presents an algorithm for the online selection of waypoints for a wildlife radio telemetry UAV, enabling the simultaneous localization of multiple VHF-tagged animals. Key components of the algorithm include the reduction of position uncertainty, optimization of mission time, energy-aware planning, consideration of potential signal loss, and maintaining a safe distance from targets to minimize disturbances and errors. Considering the performance metrics–uncertainty reduction, localization error, and mission time–the results from monte carlo simulations demonstrate that the algorithm is capable of localizing tags with high precision, accuracy, and efficiency. Also, the impact of various factors, such as the angle of the defined uncertainty wedge, the number of targets, and the number of waypoints on performance was evaluated.

Future work will involve considering the movement of animals, as this study focused on stationary targets. Additionally, a propagation model will be employed to estimate potential signal loss, replacing the simplified model currently used. Enhancing the energy model and planning the next waypoints based on real-time remaining energy are also areas for improvement. Although the computation time is not excessively long, further optimization is possible. Finally, tests will be conducted on a UAV to validate the proposed approach.

REFERENCES

[1] H. L. Larsen, K. Møller-Lassesen, E. M. E. Enevoldsen, S. B. Madsen, M. T. Obsen, P. Povlsen, D. Bruhn, C. Pertoldi, and S. Pagh, "Drone with mounted thermal infrared cameras for monitoring terrestrial mammals," *Drones*, vol. 7, no. 11, p. 680, Nov. 2023, doi: 10.3390/drones7110680.

[2] J. S. Avila-Sanchez, H. L. Perotto-Baldivieso, L. D. Massey, J. A. Ortega, L. A. Brennan, and F. Hernández, "Evaluating the use of a thermal sensor to detect small ground-nesting birds in semi-arid environments during winter," *Drones*, vol. 8, no. 2, p. 64, Feb. 2024, doi: 10.3390/drones8020064.

[3] H. Frouin-Mouy, L. Tenorio-Hallé, A. Thode, S. Swartz, and J. Urbán, "Using two drones to simultaneously monitor visual and acoustic behaviour of gray whales (*Eschrichtius robustus*) in Baja California, Mexico," *J. Experim. Mar. Biol. Ecol.*, vol. 525, Apr. 2020, Art. no. 151321, doi: 10.1016/j.jembe.2020.151321.

[4] J. Monks, H. Wills, and C. Knox, "Testing drones as a tool for surveying lizards," *Drones*, vol. 6, no. 8, p. 199, Aug. 2022, doi: 10.3390/drones6080199.

[5] R. Huang, H. Zhou, T. Liu, and H. Sheng, "Multi-UAV collaboration to survey Tibetan antelopes in hoh xil," *Drones*, vol. 6, no. 8, p. 196, Aug. 2022, doi: 10.3390/drones6080196.

[6] O. M. Cliff, R. Fitch, S. Sukkarieh, D. L. Saunders, and R. Heinsohn, "Online localization of radio-tagged wildlife with an autonomous aerial robot system," in *Robotics: Science and Systems*. Rome, Italy, 2015, doi: 10.15607/RSS.2015.XI.042.

[7] K. VonEhr, S. Hilaski, B. E. Dunne, and J. Ward, "Software defined radio for direction-finding in UAV wildlife tracking," in *Proc. IEEE Int. Conf. Electro Inf. Technol. (EIT)*, May 2016, pp. 464–469, doi: 10.1109/EIT.2016.7535285.

[8] M. W. Shafer, G. Vega, K. Rothfus, and P. Flikkema, "UAV wildlife radiotelemetry: System and methods of localization," *Methods Ecology Evol.*, vol. 10, no. 10, pp. 1783–1795, Aug. 2019, doi: 10.1111/2041-210x.13261.

[9] F. Körner, R. Speck, A. H. Göktogan, and S. Sukkarieh, "Autonomous airborne wildlife tracking using radio signal strength," in *Proc. IEEE/RSJ Int. Conf. Intell. Robots Syst.*, Taipei, Taiwan, Oct. 2010, pp. 107–112, doi: 10.1109/IROS.2010.5654385.
[10] P. Soriano, F. Caballero, and A. Ollero, "RF-based particle filter localization for wildlife tracking by using an UAV," in *Proc. Int. Symp. Robot. (ISR)*, 2009. [Online]. Available: https://www.researchgate.net/publication/268328735
[11] H. V. Nguyen, M. Chesser, L. P. Koh, S. H. Rezatofighi, and D. C. Ranasinghe, "TrackerBots: Autonomous unmanned aerial vehicle for real-time localization and tracking of multiple radio-tagged animals," *J. Field Robot.*, vol. 36, no. 3, pp. 617–635, May 2019, doi: 10.1002/rob.21857.
[12] A. T. Parameswaran et al., "Is RSSI a reliable parameter in sensor localization algorithms: An experimental study," in *Proc. IEEE Field Failure Data Anal. Workshop*, Niagara Falls, NY, USA, vol. 5, Sep. 2009.
[13] M. K. Yılmaz and H. Bayram, "Particle filter-based aerial tracking for moving targets," *J. Field Robot.*, vol. 40, no. 2, pp. 368–392, Mar. 2023, doi: 10.1002/rob.22134.
[14] N. T. Hui, E. K. Lo, J. B. Moss, G. P. Gerber, M. E. Welch, R. Kastner, and C. Schurgers, "A more precise way to localize animals using drones," *J. Field Robot.*, vol. 38, no. 6, pp. 917–928, Sep. 2021, doi: 10.1002/rob.22017.
[15] C. G. Müller, B. L. Chilvers, Z. Barker, K. P. Barnsdale, P. F. Battley, R. K. French, J. McCullough, and F. Samandari, "Aerial VHF tracking of wildlife using an unmanned aerial vehicle (UAV): Comparing efficiency of yellow-eyed penguin (*Megadyptes antipodes*) nest location methods," *Wildlife Res.*, vol. 46, no. 2, p. 145, 2019, doi: 10.1071/wr17147.
[16] B. Roberts, M. Neal, N. Snooke, F. Labrosse, T. Curteis, and M. Fraser, "A bespoke low-cost system for radio tracking animals using multi-rotor and fixed-wing unmanned aerial vehicles," *Methods Ecol. Evol.*, vol. 11, no. 11, pp. 1427–1433, Nov. 2020, doi: 10.1111/2041-210x.13464.
[17] J. Vander Hook, P. Tokekar, and V. Isler, "Cautious greedy strategy for bearing-based active localization: Experiments and theoretical analysis," in *Proc. IEEE Int. Conf. Robot. Autom.*, May 2012, pp. 1787–1792, doi: 10.1109/ICRA.2012.6225244.
[18] O. M. Cliff, D. L. Saunders, and R. Fitch, "Robotic ecology: Tracking small dynamic animals with an autonomous aerial vehicle," *Sci. Robot.*, vol. 3, no. 23, pp. 1–10, Oct. 2018, doi: 10.1126/scirobotics.aat8409.
[19] H. V. Nguyen, F. Chen, J. Chesser, H. Rezatofighi, and D. Ranasinghe, "LAVAPilot: Lightweight UAV trajectory planner with situational awareness for embedded autonomy to track and locate radio-tags," in *Proc. IEEE/RSJ Int. Conf. Intell. Robots Syst. (IROS)*, Oct. 2020, pp. 2488–2495, doi: 10.1109/IROS45743.2020.9341615.
[20] H. Bayram, N. Stefas, and V. Isler, "Aerial radio-based telemetry for tracking wildlife," in *Proc. IEEE/RSJ Int. Conf. Intell. Robots Syst. (IROS)*, Madrid, Spain, Oct. 2018, pp. 4723–4728, doi: 10.1109/IROS.2018.8594503.
[21] H. V. Nguyen, H. Rezatofighi, B.-N. Vo, and D. C. Ranasinghe, "Online UAV path planning for joint detection and tracking of multiple radio-tagged objects," *IEEE Trans. Signal Process.*, vol. 67, no. 20, pp. 5365–5379, Oct. 2019, doi: 10.1109/TSP.2019.2939076.
[22] E. Zitzler, K. Deb, and L. Thiele, "Comparison of multiobjective evolutionary algorithms: Empirical results," *Evol. Comput.*, vol. 8, no. 2, pp. 173–195, Jun. 2000.
[23] K. V. Mardia and P. E. Jupp, *Directional Statistics* (Wiley Series in Probability and Statistics). Hoboken, NJ, USA: Wiley, 2009. [Online]. Available: https://books.google.com/books?id=PTNiCm4Q-M0C
[24] J. C. Withey, T. D. Bloxton, and J. M. Marzluff, "Effects of tagging and location error in wildlife radiotelemetry studies," in *Radio Tracking and Animal Populations*, J. J. Millspaugh and J. M. Marzluff, Eds., San Diego, CA, USA: Academic, 2001, pp. 43–75, doi: 10.1016/B978-012497781-5/50004-9.
[25] V. O. Nams, "Effects of radiotelemetry error on sample size and bias when testing for habitat selection," *Can. J. Zoology*, vol. 67, no. 7, pp. 1631–1636, Jul. 1989, doi: 10.1139/z89-233.
[26] S. L. Findholt, B. K. Johnson, L. L. McDonald, J. W. Kern, and L. D. Bryant, "Adjusting for radio-telemetry error to improve estimates of habitat use," USDA Forest Service, Washington, DC, USA, Tech. Rep. PNW-RP 555, 200.
[27] M. B. Hooten, D. S. Johnson, B. T. McClintock, and J. M. Morales, *Animal Movement: Statistical Models for Telemetry Data*, 1st ed., Boca Raton, FL, USA: CRC Press, 2017, doi: 10.1201/9781315117744.
[28] H. Kwon and I. Guvenc, "RF signal source search and localization using an autonomous UAV with predefined waypoints," in *Proc. IEEE 97th Veh. Technol. Conf. (VTC-Spring)*, Jun. 2023, pp. 1–6, doi: 10.1109/VTC2023-Spring57618.2023.10200783.
[29] S. Kulkarni, V. Chaphekar, M. M. Uddin Chowdhury, F. Erden, and I. Guvenc, "UAV aided search and rescue operation using reinforcement learning," in *Proc. SoutheastCon*, vol. 2, Mar. 2020, pp. 1–8, doi: 10.1109/SoutheastCon44009.2020.9368285.
[30] D.-H. Kim, K. Lee, M.-Y. Park, and J. Lim, "UAV-based localization scheme for battlefield environments," in *Proc. IEEE Mil. Commun. Conf.*, San Diego, CA, USA, Nov. 2013, pp. 562–567, doi: 10.1109/MILCOM.2013.102.
[31] R. Saar de Moraes and E. Pignaton de Freitas, "Multi-UAV based crowd monitoring system," *IEEE Trans. Aerosp. Electron. Syst.*, vol. 56, no. 2, pp. 1332–1345, Apr. 2020, doi: 10.1109/TAES.2019.2952420.

MAHSA MOHAMMADI received the bachelor's degree in aerospace engineering from the K. N. Toosi University of Technology, Tehran, Iran, in 2020. She is currently pursuing the M.Sc. degree in mechanical engineering with Northern Arizona University, Flagstaff, AZ, USA. The focus of her thesis is on path planning for UAV-based localization systems. Her research interests include robotics, automation, control, and optimization.

MICHAEL W. SHAFER received the Ph.D. degree in mechanical engineering from Cornell University, in 2013. From 2006 to 2009, he was a Cognizant Engineer with the NASA/Caltech's Jet Propulsion Laboratory, where he designed, tested, and delivered multiple mechanisms for the Mars Curiosity Rover. He is currently an Associate Professor of mechanical engineering with Northern Arizona University. In the past, his research has focused on the optimization of piezoelectric vibrational energy harvesters, applications of vibrational energy harvesting for avian wildlife, and the use of photovoltaic power generation in the marine environment for wildlife telemetry devices. His current research interests include the intersection of robotic systems, signal processing, and resource-constrained wildlife telemetry devices.